Multiscale/Mimetic Pressure Solvers with Near-Well Grid Adaptation

Bård Skaflestad   Stein Krogstad

July 2, 2008

Abstract

Multiscale methods have proved to be an efficient means to achieving fast simulations on large reservoir models. The main characteristic of these methods is high resolution flow fields obtained at a relatively low computational cost. We are thus able to resolve large-scale flow-patterns as well as fine-scale details that would be impossible to obtain for models for which direct simulation using traditional methods would be prohibitive.

However, there are still a number of open problems in applying these methods to reservoir simulation. In particular, we observe some discrepancy in the performance of wells when compared to direct simulation on the fine-scale grid. To improve the multiscale method's predictive power for individual wells, we consider two direct opposite strategies: First, by resolving the near-well flow in the coarse grid by adaptive grid refinement in regions near wells. Second, by ensuring that near-well flow is sufficiently captured in the corresponding multiscale basis functions. For the latter strategy, we consider both adaptive alignment of the coarse pressure grid to well trajectories and an oversampling method for computing the multiscale basis functions corresponding to wells. In this paper we will study the effects of such near-well grid adaptations, and state pros and cons for the approaches considered.

Introduction

Multiscale methods for reservoir simulation have been introduced as an alternative to upscaling and as a tool for more fully incorporating important fine-scale features at low computational cost. Among the relevant approaches are multiscale finite-element methods (Hou and Wu, 1997), the multiscale finite volume method (Jenny et al., 2003) , the multiscale mixed finite element method (Chen and Hou, 2003), and the variational multiscale approach of Arbogast (2000). Here, we consider and further extend a version of the multiscale mixed finite element method (MsMFEM) (Aarnes et al., 2008), which incorporates recent mimetic finite-difference methods (Brezzi et al., 2005) as sub-grid solvers. It has been shown (Aarnes, 2004; Efendiev et al., 2006) that the accuracy of multiscale methods can be improved if global information in the form of one fine-grid velocity field computed directly on the fine grid is used in the computation of multiscale basis functions. In this paper, however, we consider only local information in the computation of basis function. As a result, the approach becomes more generic, as the initially computed set of basis functions can be utilized for a wider range of simulation scenarios. Well modeling in the context of multiscale methods has been considered by for example Chen and Yue (2003), Aarnes (2004) and Wolfsteiner et al. (2006). For MsMFEM, a robust well-modeling capability has been lacking, for instance for cases where well locations are far off the coarse block centers. In this work, we introduce special well basis functions and consider both grid adaptation and overlap/oversampling strategies for improved accuracy in the well modeling. Oversampling is a well-known approach in both upscaling (see e.g., Durlofsky (2003)) and multiscale methods (Hou and Wu, 1997; Chu et al., 2008). The oversampling approach we utilize here, is slightly different than the one suggested for the original MsMFEM (Chen and Hou, 2003), the main difference being that our approach provides a mass-conservative velocity field on the fine sub-grid. An initial study of utilizing oversampling in the MsMFEM well basis functions has been conducted by Ligaarden (2008).

The paper proceeds as follows. After introducing the model equations, we present the fine-grid discretization methodology and the linking of well equations to the hybrid linear systems. We then present the multiscale method, the multiscale block-block and well-block basis functions, and the resulting linear systems. We finally demonstrate the performance of the suggested well-representations in a few numerical experiments.

Governing Equations: We consider model equations for oil-water incompressible flow neglecting gravity and capillary pressure. Let Ω denote the computational domain with boundary Γ. The *pressure equation* gives the Darcy velocity $\vec{v}$ and pressure p for a given water saturation field s:

$$\vec{v} = -\lambda_t(s)\mathbf{K}\nabla p, \quad \nabla \cdot \vec{v} = q \text{ in } \Omega, \tag{1}$$

with boundary conditions $\vec{v} \cdot \vec{n} = f_N$ on Γ_N, and $p = p_D$ on Γ_D, where $\vec{n}$ is the outward pointing unit normal. Here $\mathbf{K}$ is the permeability tensor, $\lambda_t(s)$ is the total mobility, and q is a source term. The corresponding *saturation equation* is then given

$$\phi \frac{\partial s}{\partial t} + \nabla \cdot (f_a(s)\vec{v}) = q_a, \tag{2}$$

where ϕ is the porosity, f_a is the water fractional flow function, and q_a is the water source term. In the following, we represent wells as boundary conditions. Hence, a well w with boundary γ_w is conceptually represented as a *hole* in Ω with $\gamma_w \subset \Gamma$. We consider wells that are either pressure constrained or rate constrained, and accordingly either $\gamma_w \subset \Gamma_D$ with $p = p_D$ on γ_w or $\gamma_w \subset \Gamma_N$ with $\int_{\gamma_w} \vec{v} \cdot \vec{n} = -q_a$.

Discretization and Hybrid System

Let $\{E_i\}$ be a set of N polygonal cells constituting a grid for Ω. For a given cell E with faces e_k, $k = 1, \ldots, n_E$, let $\mathbf{v}_E$ be the vector of outward fluxes over the corresponding faces of E,

p_E the pressure at the cell center, and $\boldsymbol{\lambda}_E$ the pressures at the face centers. Many numerical methods relate these quantities through a *transmissibility* matrix $\mathbf{T}_E$ such that

$$\mathbf{v}_E = \lambda_t(s_E)\mathbf{T}_E(p_E - \boldsymbol{\lambda}_E), \tag{3}$$

where s_E is the saturation in cell E. Among the methods that can be recast in this way are the lowest-order mixed finite-element methods (MFEM) (see e.g, Brezzi and Fortin (1991)), the two-point flux-approximation (TPFA) method (see e.g., Aziz and Settari (1979)) and recent mimetic finite-difference methods (MFDM) by Brezzi et al. (2005). While MFEM and MFDM in general lead to full $\mathbf{T}_E$-matrices, the TPFA results in a diagonal $\mathbf{T}_E$, but is non-convergent for general grids. We refer to the previously mentioned references for details on the computation of $\mathbf{T}_E$ for the various methods.

For a given saturation field $\mathbf{s}$, the local equations (3) can be assembled to form a hybrid system of the form

$$\begin{pmatrix} \mathbf{B} & \mathbf{C} & \mathbf{D} \\ \mathbf{C}^\mathsf{T} & \mathbf{O} & \mathbf{O} \\ \mathbf{D}^\mathsf{T} & \mathbf{O} & \mathbf{O} \end{pmatrix} \begin{pmatrix} \mathbf{v} \\ -\mathbf{p} \\ \boldsymbol{\lambda} \end{pmatrix} = \begin{pmatrix} \mathbf{0} \\ \mathbf{q} \\ \mathbf{f} \end{pmatrix}. \tag{4}$$

Here $\mathbf{v}$ are the face out-fluxes ordered cell-wise (thus, fluxes on interior faces appear twice with opposite signs), $\mathbf{p}$ are the cell pressures and $\boldsymbol{\lambda}$ are the face pressures (without repetitions). The matrices $\mathbf{B}$ and $\mathbf{C}$ are block diagonal with blocks $(\lambda_t(s_E)\mathbf{T}_E)^{-1}$ and $(1\ 1\cdots 1)^\mathsf{T}$ (length n_E) corresponding to the cell E, respectively. Finally, each column of the matrix $\mathbf{D}$ corresponds to a unique face and has one (for boundary faces) or two (for interior faces) unit entries corresponding to the index/indices of the face in the cell-wise ordering. The right-hand side corresponds to sources $\mathbf{q}$ and flux (Neumann) boundary conditions $\mathbf{f}$. To incorporate pressure (Dirichlet) boundary conditions, one can split the vector $\boldsymbol{\lambda}^\mathsf{T} = \left(\boldsymbol{\lambda}_{I,N}^\mathsf{T}\ \boldsymbol{\lambda}_D^\mathsf{T}\right)$ and the matrix $\mathbf{D} = (\mathbf{D}_{I,N}\ \mathbf{D}_D)$ in two parts where the first corresponds to the interior and Neumann faces and the second corresponds to the Dirichlet faces. Then the hybrid system (4) reduces to

$$\begin{pmatrix} \mathbf{B} & \mathbf{C} & \mathbf{D}_{I,N} \\ \mathbf{C}^\mathsf{T} & \mathbf{O} & \mathbf{O} \\ \mathbf{D}_{I,N}^\mathsf{T} & \mathbf{O} & \mathbf{O} \end{pmatrix} \begin{pmatrix} \mathbf{v} \\ -\mathbf{p} \\ \boldsymbol{\lambda}_{I,N} \end{pmatrix} = \begin{pmatrix} -\mathbf{D}_D\boldsymbol{\lambda}_D \\ \mathbf{q} \\ \mathbf{f}_{I,N} \end{pmatrix}. \tag{5}$$

Since the inverse of $\mathbf{B}$ is block diagonal with blocks $\lambda_t(s_E)\mathbf{T}_E$, the flux vector $\mathbf{v}$ can efficiently be eliminated from the system (5) to obtain

$$\begin{pmatrix} \boldsymbol{\Lambda} & -\mathbf{M} \\ -\mathbf{M}^\mathsf{T} & \mathbf{S} \end{pmatrix} \begin{pmatrix} \mathbf{p} \\ \boldsymbol{\lambda}_{I,N} \end{pmatrix} = \begin{pmatrix} \hat{\mathbf{q}} \\ \hat{\mathbf{f}} \end{pmatrix}, \tag{6}$$

where $\boldsymbol{\Lambda} = \mathbf{C}^\mathsf{T}\mathbf{B}^{-1}\mathbf{C}$, $\mathbf{M} = \mathbf{C}^\mathsf{T}\mathbf{B}^{-1}\mathbf{D}_{I,N}$, $\mathbf{S} = \mathbf{D}_{I,N}^\mathsf{T}\mathbf{B}^{-1}\mathbf{D}_{I,N}$, $\hat{\mathbf{q}} = \mathbf{q} + \mathbf{C}^\mathsf{T}\mathbf{B}^{-1}\mathbf{D}_D\boldsymbol{\lambda}_D$, and finally $\hat{\mathbf{f}} = \mathbf{f}_{I,N} + \mathbf{D}_{I,N}^\mathsf{T}\mathbf{B}^{-1}\mathbf{D}_D\boldsymbol{\lambda}_D$. In the system (6), the matrix $\boldsymbol{\Lambda}$ is diagonal (and thus easily invertible), and by eliminating $\mathbf{p}$, one obtains the SPD system

$$\left(\mathbf{S} - \mathbf{M}^\mathsf{T}\boldsymbol{\Lambda}^{-1}\mathbf{M}\right)\boldsymbol{\lambda}_{I,N} = \hat{\mathbf{f}} + \boldsymbol{\Lambda}^{-1}\hat{\mathbf{q}}. \tag{7}$$

After solving (7), the cell pressures $\mathbf{p}$ and face fluxes $\mathbf{v}$ are obtained through back substitution.

Well Modeling

Since typical wells in reservoirs have small diameters compared to the size of the simulation cells, it is common to employ a well index (productivity index) WI to relate the local flow rate q to the difference in well pressure p_w and numerically computed pressure p_E in the perforated grid-cell by

$$-q = \lambda_t(s_E)\,WI(p_E - p_w). \tag{8}$$

Commonly used is Peaceman's well index (Peaceman, 1983), which for a vertical well in a Cartesian cell with dimensions $\Delta x \times \Delta y \times \Delta z$ is given

$$WI = \frac{2\pi k \Delta z}{\ln(r_0/r_w)}. \qquad (9)$$

For isotropic media, k is given by $\mathbf{K} = k\mathbf{I}$, and $r_0 = 0.14(\Delta x^2 + \Delta y^2)^{\frac{1}{2}}$. Here r_0 is the *effective well-cell radius*, and can be interpreted as (ideally) the radius at which the actual pressure equals the numerically computed pressure. The validity of the Peaceman well-index decreases rapidly with increasing near-well heterogeneity and grid skewness. It is also important to note that the Peaceman well-index is developed for the TPFA-method and is not valid for other methods (as MFEM with exact integration or MFDMs in general). We refer to Ligaarden (2008) for a study on extension of Peaceman's results to methods other than TPFA. We hence forth assume that sensible well-indices are given, and discuss the inclusion of wells in the linear system (4).

Consider a system containing N_w wells $w_1, \ldots, w_{N_w}$. For a well w_k, let n_k be the number of cells perforated by the well, and denote these cells by E_{k_i}, $i = 1, \ldots, n_k$. Furthermore, let WI_i^k be the well index corresponding to the perforation of well w_k in cell E_{k_i}. The set of equations for all wells is then given, for $k = 1, \ldots, N_w$

$$-q_i^k = \lambda_t(s_{k_i}) WI_i^k (p_{E_{k_i}} - p_{w_k}), \quad i = 1, \ldots, n_k,$$
$$q_{\text{tot}}^k = \sum_{i=1}^{n_k} q_i^k. \qquad (10)$$

Assuming zero flux boundary conditions everywhere except at wells and no additional sources, the equations (10) are coupled to the system (4) to form the linear system

$$\begin{pmatrix} \mathbf{B} & \mathbf{O} & \mathbf{C} & \mathbf{D} & \mathbf{O} \\ \mathbf{O} & \mathbf{B}_w & \mathbf{C}_w & \mathbf{O} & \mathbf{D}_w \\ \mathbf{C}^\mathsf{T} & \mathbf{C}_w^\mathsf{T} & \mathbf{O} & \mathbf{O} & \mathbf{O} \\ \mathbf{D}^\mathsf{T} & \mathbf{O} & \mathbf{O} & \mathbf{O} & \mathbf{O} \\ \mathbf{O} & \mathbf{D}_w^\mathsf{T} & \mathbf{O} & \mathbf{O} & \mathbf{O} \end{pmatrix} \begin{pmatrix} \mathbf{v} \\ -\mathbf{q}_w \\ -\mathbf{p} \\ \boldsymbol{\lambda} \\ \mathbf{p}_w \end{pmatrix} = \begin{pmatrix} \mathbf{0} \\ \mathbf{0} \\ \mathbf{0} \\ \mathbf{0} \\ -\mathbf{q}_{w,\text{tot}} \end{pmatrix}. \qquad (11)$$

Here the matrices $\mathbf{B}_w$, $\mathbf{C}_w$ and $\mathbf{D}_w$ are given

$$\mathbf{B}_w = \begin{pmatrix} \mathbf{B}_1 & & \mathbf{O} \\ & \ddots & \\ \mathbf{O} & & \mathbf{B}_{N_w} \end{pmatrix}, \quad \mathbf{C}_w = \begin{pmatrix} \mathbf{C}_1 \\ \vdots \\ \mathbf{C}_{N_w} \end{pmatrix}, \quad \mathbf{D}_w = \begin{pmatrix} \mathbf{d}_1 & & \mathbf{0} \\ & \ddots & \\ \mathbf{0} & & \mathbf{d}_{N_w} \end{pmatrix}, \qquad (12)$$

where $\mathbf{B}_k$ is the $n_k \times n_k$ diagonal matrix with $\{\mathbf{B}_k\}_{ii} = (\lambda_t(s_{k_i}) WI_i^k)^{-1}$; $\mathbf{C}_w$ is the sparse $n_w \times N$ matrix having unit entries in positions (i, k_i), $i = 1, \ldots, n_k$; and finally $\mathbf{d}_w$ is a $n_k \times 1$ vector with all entries equal to one. The vectors $\mathbf{q}_w$, $\mathbf{p}_w$, and $\mathbf{q}_{w,\text{tot}}$ in (11) contain the local well rates, well pressures, and total well rates, respectively. We impose the well boundary condition either as rate constrained (Neumann), where q_{tot}^k is given, or pressure constrained (Dirichlet), where p_{w_k} is given. For pressure constrained wells, the system is reduced according to (5).

Multiscale Mixed/Mimetic Discretizations

In the current MsMFEM (Aarnes et al., 2008) we consider two grids, where the coarse grid consist of blocks Ω_i containing a connected set of cells from the underlying fine grid. A fine grid velocity field is sought through a linear combination of initially computed coarse grid basis functions obtained by a local fine-grid flow problem.

Basis functions: We use two sets of basis functions, one set corresponding to the block-block interfaces, and one set for the well-block interfaces. Consider two neighboring blocks Ω_i and

Ω_j, and let Ω_{ij} be a neighborhood containing Ω_i and Ω_j. Then we define the basis function $\vec{\psi}_{ij}$ by

$$\vec{\psi}_{ij}(\vec{x}) = -\mathbf{K}\nabla p_{ij}(\vec{x}), \quad \nabla \cdot \vec{\psi}_{ij}(\vec{x}) = \begin{cases} \omega_i(\vec{x}) & \text{if } \vec{x} \in \Omega_i, \\ -\omega_j(\vec{x}) & \text{if } \vec{x} \in \Omega_j, \\ 0 & \text{otherwise,} \end{cases} \quad \text{in } \Omega_{ij}, \quad (13)$$

and $\vec{\psi}_{ij} \cdot \vec{n} = 0$ on $\partial\Omega_{ij}$. In (13), ω_i is a weighting function of unit integral over Ω_i. In particular we choose

$$\omega_i(\vec{x}) = \frac{\text{trace}(\mathbf{K}(\vec{x}))}{\int_{\Omega_i} \text{trace}(\mathbf{K}(\vec{x})) \, \mathrm{d}\vec{x}}, \quad (14)$$

which has been shown to give better results than for instance using a uniform source (Aarnes et al., 2006). If $\Omega_{ij} \neq \Omega_i \cup \Omega_j$, we say that the basis function is computed using overlap or oversampling. Next, we discuss basis functions corresponding to the well-block interfaces. Assume a block Ω_i is perforated by a well w_k with boundary γ_{w_k}, and let Ω_i^k be a neighborhood containing Ω_i. Furthermore, let $\gamma_i^k = \gamma_{w_k} \cap \partial\Omega_i^k$. Then, we define the basis function $\vec{\psi}_i^k$ by

$$\vec{\psi}_i^k(\vec{x}) = -\mathbf{K}\nabla p_i^k(\vec{x}), \quad \nabla \cdot \vec{\psi}_i^k(\vec{x}) = \begin{cases} -\omega_i(\vec{x}) & \text{if } \vec{x} \in \Omega_i, \\ 0 & \text{otherwise,} \end{cases} \quad \text{in } \Omega_i^k, \quad (15)$$

with boundary conditions $p_i^k = $ constant on γ_i^k and $\vec{\psi}_i^k \cdot \vec{n} = 0$ on $\partial\Omega_i^k \setminus \gamma_i^k$. As for the block-block basis functions, overlap is used whenever $\Omega_i^k \neq \Omega_i$.

Discretization: Let $\boldsymbol{\psi}_{ij}$ denote the vector of fluxes defined on the set of cell-wise ordered faces in the fine grid obtained from solving the subset of the system (4) corresponding to Equation (13) with given source and boundary conditions. Similarly let $\boldsymbol{\psi}_i^k$ and $\mathbf{q}_i^k$ represent face fluxes and well rates (defined on the total set of fine grid perforations) in the numerical solution of (15) obtained by solving the corresponding subset of (11) with prescribed boundary conditions and source. We next describe the multiscale hybrid system. For the block-block basis functions, define the splitting $\boldsymbol{\psi}_{ij} = \boldsymbol{\psi}_{ij}^H - \boldsymbol{\psi}_{ji}^H$ by

$$\boldsymbol{\psi}_{ij}^H(E) = \begin{cases} \boldsymbol{\psi}_{ij}(E) & \text{if } E \in \Omega_{ij} \setminus \Omega_j, \\ 0 & \text{otherwise,} \end{cases}, \quad \boldsymbol{\psi}_{ji}^H(E) = \begin{cases} -\boldsymbol{\psi}_{ij}(E) & \text{if } E \in \Omega_j, \\ 0 & \text{otherwise.} \end{cases} \quad (16)$$

Furthermore, arrange all the *hybrid* basis functions $\boldsymbol{\psi}_{ij}^H$ as columns in a matrix $\boldsymbol{\Psi}$, all $\boldsymbol{\psi}_i^k$ as columns in a matrix $\boldsymbol{\Psi}_w$, and all basis well-rates $\mathbf{q}_i^k$ in a matrix $\mathcal{R}_w$. The resulting multiscale hybrid system now takes the form

$$\begin{pmatrix} \mathbf{B}_{11} & \mathbf{B}_{12} & \mathbf{C} & \mathbf{D} & \mathbf{O} \\ \mathbf{B}_{12}^\mathsf{T} & \mathbf{B}_{22} & \mathbf{C}_w & \mathbf{O} & \mathbf{D}_w \\ \mathbf{C}^\mathsf{T} & \mathbf{C}_w^\mathsf{T} & \mathbf{O} & \mathbf{O} & \mathbf{O} \\ \mathbf{D}^\mathsf{T} & \mathbf{O} & \mathbf{O} & \mathbf{O} & \mathbf{O} \\ \mathbf{O} & \mathbf{D}_w^\mathsf{T} & \mathbf{O} & \mathbf{O} & \mathbf{O} \end{pmatrix} \begin{pmatrix} \mathbf{v} \\ -\mathbf{q}_w \\ -\mathbf{p} \\ \boldsymbol{\lambda} \\ \mathbf{p}_w \end{pmatrix} = \begin{pmatrix} \mathbf{0} \\ \mathbf{0} \\ \mathbf{0} \\ \mathbf{0} \\ -\mathbf{q}_{w,\text{tot}} \end{pmatrix}, \quad (17)$$

where $\mathbf{C}$, $\mathbf{C}_w$, $\mathbf{D}$, and $\mathbf{D}_w$ are constructed from the coarse grid analogous to (11). Letting $\mathbf{B}^f$ and $\mathbf{B}_w^f$ denote the fine-grid system matrices in (11), the three $\mathbf{B}_{ij}$-matrices are given $\mathbf{B}_{11} = \boldsymbol{\Psi}^\mathsf{T} \mathbf{B}^f \boldsymbol{\Psi}$, $\mathbf{B}_{12} = \boldsymbol{\Psi}^\mathsf{T} \mathbf{B}^f \boldsymbol{\Psi}_w$, and finally $\mathbf{B}_{22} = \boldsymbol{\Psi}_w^\mathsf{T} \mathbf{B}^f \boldsymbol{\Psi}_w + \mathcal{R}_w^\mathsf{T} \mathbf{B}_w^f \mathcal{R}_w$. If the basis functions are computed without overlap, the $\mathbf{B}$-part of (17) is block diagonal with respect to the coarse blocks Ω_i, and thus (17) can efficiently be reduced to a SPD system for $\boldsymbol{\lambda}$ and the unknown entries of $\mathbf{p}_w$. When overlap is used, one is in general better off using a mixed formulation of the system (17). Having obtained a solution to (17), the fine-grid face-flux and fine-grid well-rate approximations are given by $\mathbf{v}^f = \boldsymbol{\Psi}\mathbf{v} + \boldsymbol{\Psi}_w \mathbf{q}_w$ and $\mathbf{q}_w^f = \mathcal{R}_w \mathbf{q}_w$, respectively.
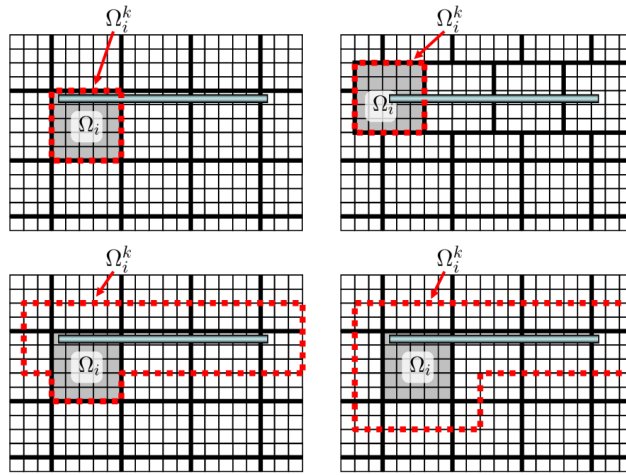
Figure 1: Four approaches for handling wells in a multiscale basis function. Standard (top left), adapted around well (top right), well oversampling (bottom left), and both well and block oversampling (bottom right).

Numerical Experiments

In this section we present numerical experiments exploring various strategies for improved well-modeling in the current multiscale methodology. In the considered strategies, we either alter and adapt the coarse grid or use overlap/oversampling. In particular we consider five distinct approaches:

- **Standard:** The coarse grid is a general, logically Cartesian partitioning of the fine grid, and both the block-block and well-block basis functions are computed without overlap, see Figure 1 top-left illustration. This approach is labeled *MS* in plots.

- **Adapted around wells:** The initial partitioning is altered such that the coarse grid follows the well trajectory, see Figure 1 top-right illustration. Labeled *MS_adapt* in plots.

- **Adapted and refined around wells:** The adapted well-blocks are further subdivided into smaller blocks. Labeled *MS_refine* in plots.

- **Well oversampling:** The support domain for every well-block basis function is enlarged to include a certain fine-cell radius around the whole well, see Figure 1 bottom-left illustration. Labeled *MS_ow* in plots.

- **Well and block oversampling:** In addition to well oversampling, the support domains for both well-block and block-block basis functions are enlarged to include a given fine-cell radius around the coarse blocks, see Figure 1 bottom-right illustration. Labeled *MS_owb* in plots.

In the numerical examples, we employ rate-constrained injectors and pressure-constrained producers, all producing at equal pressure. Denote by I and P the set of injectors and producers, respectively. Futhermore, for $w \in I$ let Δp_w denote the pressure drop from the well to the producers, and for $w \in P$ let q_w denote the total production rate. We compare the obtained well pressures and rates to a reference solution obtained by solving the fine-grid equations using the error measures

$$e_p = \Big(\sum_{w \in I} \Delta p_w^{\mathrm{ref}} \Big)^{-1} \sum_{w \in I} |\Delta p_w^{\mathrm{ref}} - \Delta p_w|, \quad e_r = \Big(\sum_{w \in P} q_w^{\mathrm{ref}} \Big)^{-1} \sum_{w \in P} |q_w^{\mathrm{ref}} - q_w|. \quad (18)$$

Example 1: In this numerical example we consider a $60 \times 220 \times 10$ Cartesian grid with 67 permeability realizations sampled from the Tenth SPE Comparative Solution Project (Christie and Blunt, 2001). The first 26 realizations are log-normally distributed, while the remaining 41 contain high-permeable channels. We consider two well-configurations depicted in Figure 2,
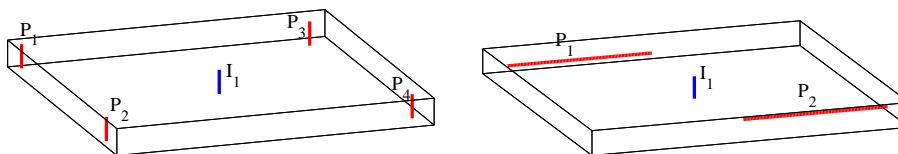
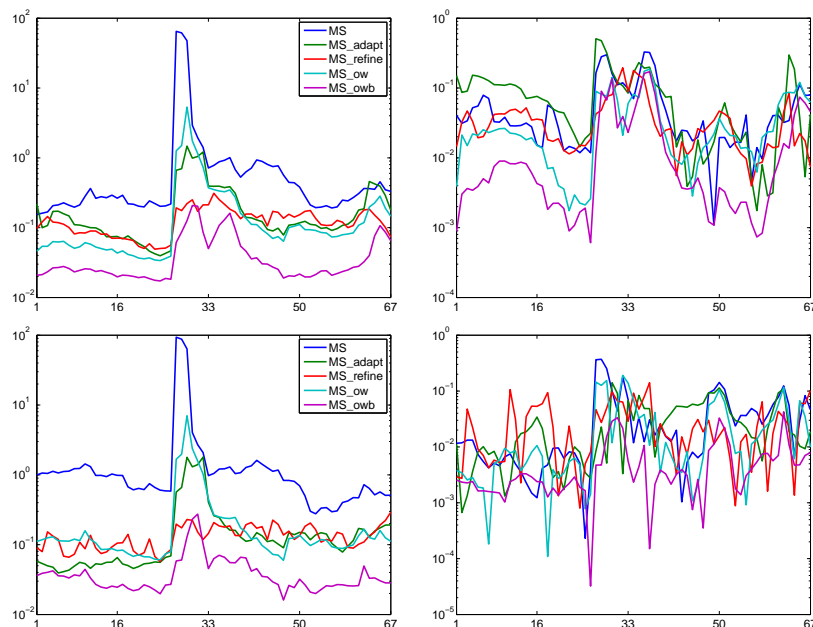Figure 2: Well configurations of Example 1.

Figure 3: Relative error in pressure (left) and total rates (right) for all 67 cases with well configuration 1 (top) and configuration 2 (bottom).

both having a single vertical injector close to the center of the model. The first configuration has four vertical producers close to the corners, while the second has two long horizontal producers perforating 100 fine cells each. In this example, we consider only single-phase flow, and thus measure the ability of the multiscale approaches to reproduce the velocity field obtained by solving the fine-grid pressure equation. The multiscale methods use a coarse grid of size $6 \times 22 \times 1$, thus an upscaling factor of 1000. The near-well refinement approach uses a $3 \times 3 \times 2$ coarse block subdivision, and the oversampling approaches utilize an overlap of 5 fine cells around the coarse blocks/wells. All fine grid computaions are performed using a MFDM. The error measures (18) for the two configurations on the 67 realizations are plotted in Figure 3. It is apparent that both grid adaptation and oversampling improves the pressure solution compared to standard MsMFEM. Accordingly, a large amount of the error committed in the standard MsMFEM is near the wells. However, further improvements are achieved by using overlap for all basis functions as can be seen in Figure 3. For the error in total rates, the improvements are not as apparent as for the pressure, as all methods perform reasonably good with a worst-case average error for each well of about $10\,\%$.

Example 2: In this example we consider a synthetic model containing about $550\,000$ fine cells with a log-normally distributed permeability field ranging about 4 orders of magnitude horizontally and a constant vertical to horizontal anisotropy ratio of 0.1. Three vertical injectors and three close to horizontal producers are situated in the model as depicted in Figure 4. The model is initially filled with oil, and the three injectors all inject water at equal and constant rates. The water-oil mobility ratio is taken to be 10, and we use quadratic relative permeability curves. The pressure and saturation equations are solved sequentially using the various multiscale ap-
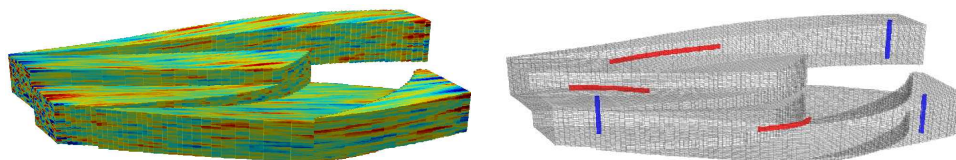
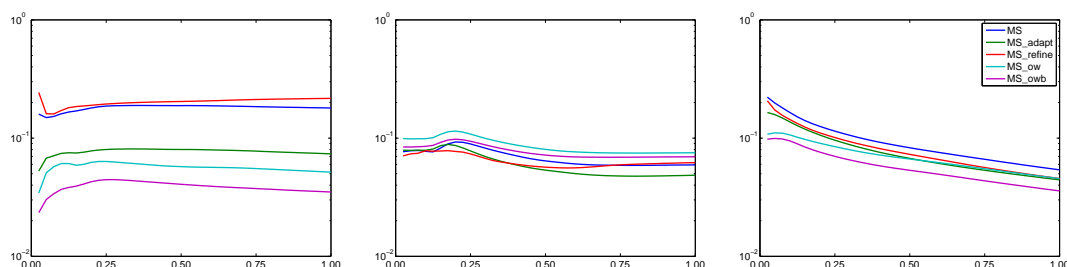Figure 4: Permeability field and well configuration of Example 2.

Figure 5: Realtive errors for numerical Example 2 in pressure (left), total rates (middle) and saturation (right).

proaches and an upstream weighted implicit finite volume scheme, respectively. Again, the upscaling factor is about 1000. All fine grid computaions are performed using a TPFA method. In Figure 5 the error measures for pressure drop, total rates and saturation are plotted as a function of time measured in PVI (pore volumes injected). The satuation error is measured as the integrated saturation discrepancy devided by total amount of injected water. Again, substantial impovements in the pressure drop is observed (except for the *MS_refine*-case), while errors in rates and saturation are fairly equal for all the multiscale approaces.

Concluding remarks

We have presented several strategies for improved well modeling in the MsMFEM. Both coarse grid adaptation and basis overlap improves the multiscale pressure solution, while a similar improvement for rates are not as apparent. The grid adaptation technique leads to a SPD system and is thus efficient for a given set of wells. In the overlap approches however, one in general needs to solve a saddle-point problem. However, the latter approach is more flexible with respect to simulation scenarios, for instance as in well placement optimization since *moving* a well only would require computing new well basis functions, and not altering the coarse grid.

In this paper we have considered rate-driven incompressible flow, and one may argue that an accurate pressure field in this context is of secondary importance. For more complex physics, however, the accuracy of the pressure becomes crutial, and in this respect, we believe that the proposed approaches will contribute to the current development of a black-oil MsMFEM pressure solver.

References

Aarnes, J.E. [2004] On the use of a mixed multiscale finite element method for greater flexibility and increased speed or improved accuracy in reservoir simulation. *Multiscale Model. Sim.*, **2**(3), 421–439.

Aarnes, J.E., Krogstad, S., and Lie, K.A. [2006] A hierarchical multiscale method for two-phase flow based upon mixed finite elements and nonuniform coarse grids. *Multiscale Model. Sim.*, **5**(2), 337–363.

Aarnes, J.E., Krogstad, S., and Lie, K.A. [2008] Multiscale mixed/mimetic methods on corner-point grids. *Comput. Geosci., to appear.*

Arbogast, T. [2000] Numerical Subgrid Upscaling of Two-Phase Flow in Porous Media. In: Chen, Z., Ewing, R.E., and Shi, Z.C. (Eds.) *LNP Vol. 552: Numerical Treatment of Multiphase Flows in Porous Media*. 35–49.

Aziz, K. and Settari, A. [1979] *Petroleum reservoir simulation*. Computational Mathematics, Springer Verlag, New York.

Brezzi, F. and Fortin, M. [1991] *Mixed and hybrid finite element methods*. Computational Mathematics, Springer Verlag, New York.

Brezzi, F., Lipnikov, K., and Simoncini, V. [2005] A family of mimetic finite difference methods on polygonal and polyhedral meshes. *Math. Mod. Meth. Appl. S.*, **15**(10), 1533–1551.

Chen, Z. and Hou, T. [2003] A mixed multiscale finite element method for elliptic problems with oscillating coefficients. *Math. Comp.*, **72**, 541–576.

Chen, Z.M. and Yue, X.Y. [2003] Numerical homogenization of well singularities in the flow transport through heterogeneous porous media. *Multiscale Model. Sim.*, **1**, 260–303.

Christie, M.A. and Blunt, M.J. [2001] Tenth SPE comparative solution project: A comparison of upscaling techniques. *SPE Reserv. Eval. Eng.*, **4**(4), 308–317.

Chu, J., Efendiev, Y., Ginting, V., and Hou, T.Y. [2008] Flow based oversampling technique for multiscale finite element methods. *Adv. Water. Resour.*, **31**, 599–608.

Durlofsky, L.J. [2003] Upscaling of geocellular models for reservoir flow simulation: a review of recent progress. In: *Proceedings of the 7th International Forum on Reservoir Simulation*.

Efendiev, Y., Ginting, V., Hou, T., and Ewing, R. [2006] Accurate multiscale finite element methods for two-phase flow simulations. *J. Comput. Phys.*, **220**, 155–174.

Hou, T. and Wu, X.H. [1997] A multiscale finite element method for elliptic problems in composite materials and porous media. *J. Comput. Phys.*, **134**, 169–189.

Jenny, P., Lee, S.H., and Tchelepi, H.A. [2003] Multi-scale finite-volume method for elliptic problems in subsurface flow simulation. *J. Comput. Phys.*, **187**(1), 47–67.

Ligaarden, I.S. [2008] *Well Models for Mimetic Finite Difference Methods and Improved Representation of Wells in Multiscale Methods*. Master Thesis, University of Oslo.

Peaceman, D.W. [1983] Interpretation of well-block pressures in numerical reservoir simulation with non-square grid blocks and anisotrpoic permeability. *SPE, Trans. AIME*, **275**, 10–22.

Wolfsteiner, C., Lee, S.H., and Tchelepi, H.A. [2006] Well modeling in the multiscale finite volume method for subsurface flow simulation. *Multiscale Model. Sim.*, **5**, 900–917.